Green Chemistry Letters and Reviews

ISSN: (Print) (Online) Journal homepage: https://www.tandfonline.com/loi/tgcl20

Purification technology for renewable production of fuel from methanolysis of waste sunflower oil in the presence of high silica zeolite beta

Leila Fereidooni, Mojtaba Enayati & Alireza Abbaspourrad

To cite this article: Leila Fereidooni, Mojtaba Enayati & Alireza Abbaspourrad (2021) Purification technology for renewable production of fuel from methanolysis of waste sunflower oil in the presence of high silica zeolite beta, Green Chemistry Letters and Reviews, 14:1, 2-14, DOI: 10.1080/17518253.2020.1856426

To link to this article: https://doi.org/10.1080/17518253.2020.1856426

Published online: 30 Dec 2020.

GREEN CHEMISTRY LETTERS AND REVIEWS
2021, VOL. 14, NO. 1, 2–14
https://doi.org/10.1080/17518253.2020.1856426

Taylor & Francis
Taylor & Francis Group

LETTER

OPEN ACCESS Check for updates

Purification technology for renewable production of fuel from methanolysis of waste sunflower oil in the presence of high silica zeolite beta

Leila Fereidooni[a], Mojtaba Enayati[b] and Alireza Abbaspourrad[b]

[a]Department of Applied Chemistry, Faculty of Chemistry, Islamic Azad University, Tehran, Iran; [b]Department of Food Science, Cornell University, Ithaca, NY, USA

ABSTRACT

Waste sunflower oil (WSO) can be easily produced as a reliable resource sustainable for multifunctional applications. WSO methanolysis in the presence of high silica zeolite beta (HSZB) treated with KOH as a catalyzer in a trans-esterification reaction was used for the fatty acid methyl ester (FAME) synthesis. Tetrahydrofuran (THF) as a co-solvent of 20 wt.% was added for mass transfer intensification. Conversion efficiency of 96.5% was obtained within 4 h reaction time of the reflux reaction, methanol:oil ratio of 9:1, 2 wt.% of catalyst and agitation speed of 300 rpm. Furthermore, these KOH treated HSZB catalysts still exhibit acceptable sustainability and appropriate catalysis in the trans-esterification after three consecutive cycling. It is concluded that K_2O existing in the pores and the defect sites of the alkali-treated HSZB can be supplied to the surface of the catalysts structure during the trans-esterification in three consecutive rounds to result in 66.3% percentage of conversion.

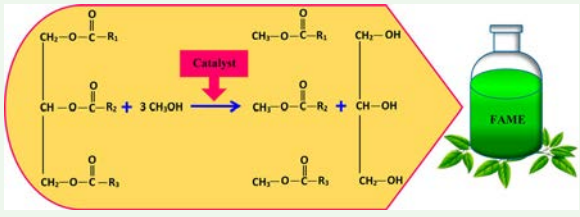

ARTICLE HISTORY
Received 25 November 2017
Accepted 20 November 2020

KEYWORDS
Trans-esterification; waste sunflower oil; fatty acids methyl esters; high silica zeolite beta

1. Introduction

Renewable fuel has greatly attracted the attention of researchers to be used instead of conventional diesel to decrease environmental pollutions and the relative negative effects (*1*). Biodiesel as a biofuel consists of mono alkyl esters which are attained by trans-esterification of animal fat or plant oil with alcohols of short chain such as ethanol or methanol (*2*). Methanolysis or trans-esterification is considered as the best technique for reducing viscosity of plant oils (*3*). However, waste oil is considerably cheaper than pure refined vegetable oils; it is noteworthy that disposal of waste materials like waste cooking may cause health-related risks and the environmental risks (*4,5*). Waste oil, as a plentiful and sustainable feedstock, can be used for biodiesel production (*6*), but the extensive pretreatments affect its economic viability since the economic aspects of biodiesel production are of considerable importance for its sustainable preparation (*7*).

Utilization of heterogeneous catalysts is considered as an important factor for the commercial production of biodiesel (*8,9*). Due to a variety of advantages such as less corrosion, convenient handling and separation, reusability and less amount of toxic wastes, heterogeneous catalysts are considered as efficient alternatives to homogeneous catalyst (*10*). Production of zeolite as a catalyst has increasingly improved in recent years (*11*). In general, zeolites are based on the structure of three-dimensional network of an aluminum and silicon tetrahedral as TO_4 (T = Co, Fe, Si, B, Al, Ge, P) linked by shared oxygen atoms (*12*). The positive charge of aluminum is lower than silicon's positive charge. Consequently, the frame has generally a net negative charge balanced by exchangeable (e.g. Mg^{2+}, Na^{+}, Ca^{2+} and K^{+}). As a result, this negative surface charge gives zeolite an excellent affinity for cationic ions (*13,14*). A rich variety of zeolite types have been considered and used for waste oils trans-esterification including KOH/

CONTACT Alireza Abbaspourrad alireza@cornell.edu

bentonite zeolite (15), NaOH/bentonite (16,17), natural zeolite from Pacitan Indonesia (18), zeolite tuff (19), KOH/ZSM5 zeolite (20), clinoptilolite zeolite (21), etc. High silica zeolite beta (HSZB) is one of the most widely used porous materials because of large cages and pores, three-dimensional channel networks and high Si/Al ratio (22). The main advantage of using heterogeneous catalyst is minimizing the problems associated with homogeneous catalyst which are recycling and regeneration, catalyst separation and soap formation (21,23). As a consequence, the extensive product purification steps and disposal problems are eliminated to offer an economical pathway for production of biodiesel.

The present study aims at developing a new heterogeneous catalyst from HSZB for fatty acid methyl ester (FAME) production from waste sunflower oil (WSO). The heterogeneous zeolite beta catalyst is economically feasible, technically applicable and environmentally friendly with a lowest level of complexity system in preparing and using the product. In this research, the heterogeneous alkaline zeolite beta catalyst was loaded and prepared to produce FAME through the trans-esterification reaction resulted from reflux. Catalyst properties have been analyzed by scanning electron microscopy (SEM), energy-dispersive X-ray (EDX), Fourier transform infrared (FT-IR), Brunauer–Emmett–Teller (BET) and X-ray diffraction (XRD) analyses. In this research, the used catalyst was prepared from impregnation of HSZB by KOH solution. The characteristics of the texture of this catalyst was examined for understanding its structure, considering active sites in the catalyst, and its sustainability in the study to provide proper conditions for trans-esterification reaction of the WSO using the advantages of the catalyst. The prepared zeolite beta catalysts were used for trans-esterification of WSO to biodiesel production. Also parameters like catalyst weight percent, alcohol:oil molar ratio, temperature, different percentages of co-solvent and time were tested. At the end, restoring the intended catalyst has been surveyed in terms of the obtained optimized ratios.

2. Experimental

2.1. Materials and methods

HSZB was obtained from Delta Factory (Iran). For the trans-esterification, WSO was collected from the central restaurant of a big hospital in Tehran. The collected waste oil has been pretreated before doing work experiment. The method used by Tanawannapong et al. was applied to use WSO (24). To remove fine particles and suspended matter in the WSO, it was first filtered and then, to reduce the acid value, it went through a 2 h reaction with sulfuric acid in 1 wt.%. To determine the acid value, the product was titrated. WSO with an acid value of 0.38 $mg_{KOH}\ g^{-1}$ matching with a free fatty acid (FFA) level of 0.19% and initial saponification value of 149.58 $mg_{KOH}\ mg_{Oil}^{-1}$ was used.

Using a Karl–Fischer titration method, the amount of water in waste oil was measured to be 0.01% (w/w). Waste oil molecular weight was 863.48 g mol^{-1}, measured based on saponification value. Equations (1) and (2) were used to calculate the acid value and FFA, respectively (25). The oil was taken in a conical flask and dissolved in 50 mL of 2-propanol by gradually heating it. Using phenolphthalein as indicator, the obtained solution was titrated against 0.1 N KOH until a slight pink color was seen. Based on Equation (2), the FFA content is calculated as half of acid value.

$$\text{Acid value} = \frac{N \times V \times 56}{W}, \tag{1}$$

$$\text{FFA} = \frac{\text{acid value}}{2}, \tag{2}$$

where N represents normality titrant (KOH), V stands for consumed volume titrant (mL), 56 is the equivalent weight of KOH and W is the weight of fatty acid (g).

Potassium hydroxide (KOH) (99%), tetrahydrofuran (THF) ($(CH_2)_3CH_2O$) (≥99.8%), sodium sulfate (Na_2SO_4) (≥99%), hydrogen peroxide (H_2O_2) (35%), sulfuric acid (H_2SO_4) (95–97%) and methanol (CH_3OH) (99.5%) were supplied by Merck Company (Germany). Oven Pars 120 KET (Iran) and heater magnetic stirrers Heidolph (Germany) were used in this research.

2.2. Characterization

FT-IR spectra (Nicolet 5700) were measured in the 400–4000 cm^{-1} range. All spectra were obtained with a resolution of 4 cm^{-1} and accumulation of 64 scans. The fine powder solid substances were mixed with potassium bromide (KBr) and pressed. The samples' XRD were measured with a Philips X'pert PRO equipped with a Cu Kα radiation (wavelength = 0.154187 nm) at the scan speed of 0.03° s^{-1} ($2\theta = 5$–65°). SEM on a Cam Scan apparatus with the applied voltage of 20 kV was used to observe the morphology of the samples. To determine the composition of the compounds, EDX (Flash & Bruker 6120) data were collected. BELMax (BEL, Japan) with nitrogen adsorption gas at 77 K and a pressure $P\,P_0^{-1} = 1 \times 10^{-8}$ was used to carry out specific surface area (BET) of the prepared samples (0.5 g powder). The gas chromatography–mass

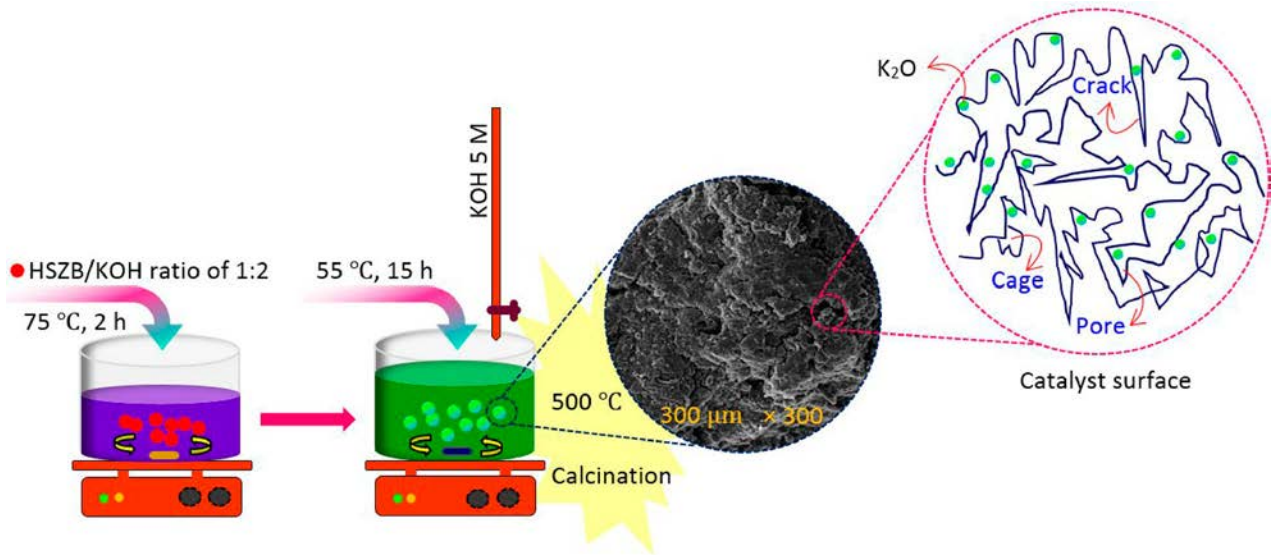

Figure 1. Schematic of the preparation method and activation of the HSZB structure by K_2O.

spectrometry (GC–MS) was equipped with flame ionization detector (FID) detector and biodiesel column model of WAXCP 9080 with an internal diameter of 0.25 mm and 30 m length. The carrier gas was helium. The column temperature was 60°C at the beginning, constant for 2 min, reaching 210° with a slope of 10° min^{-1} and immediately reached 230°C with a slope of 5° min^{-1} and kept for 10 min at the final temperature.

2.3. Procedure

Considering the loss of catalytic activity caused by poisoning, the like phenomenon is an important aspect when using heterogeneous catalysts. It is mostly approved that when contacting with air, heterogeneous catalysts may lose their activity due to adsorption of CO_2 and H_2O onto the solid surface (*26*,*27*). To remove the organic impurities, HSZB was treated with H_2O_2 30% solution. Then, H_2O_2 solution was disappeared by hot water several times. In the next stage, to get rid of moisture from HSZB, the purified HSZB was dried in an oven at 120°C for 10 h. Finally, a hammer was used to pulverize the dried zeolite. The conventional process of hydrothermal treatment with KOH was adopted for the synthesis of potassic HSZB. First, 7.5 g of the HSZB sample was incorporated in an alkaline solution (15 g of KOH + 100 mL distilled water) with HSZB/KOH ratio 1:2, under stirring (300 rpm) at a reaction temperature of 75°C for 2 h. The resulting mixture was dried for two days at room temperature. After that, the product obtained in the first stage reacted with potassic solution of 5 M KOH at 55°C, with a reaction time of 15 h, and then calcined for 4 h at 500°C (Figure 1). Different weight percent of the catalyst based on the oil weight percent

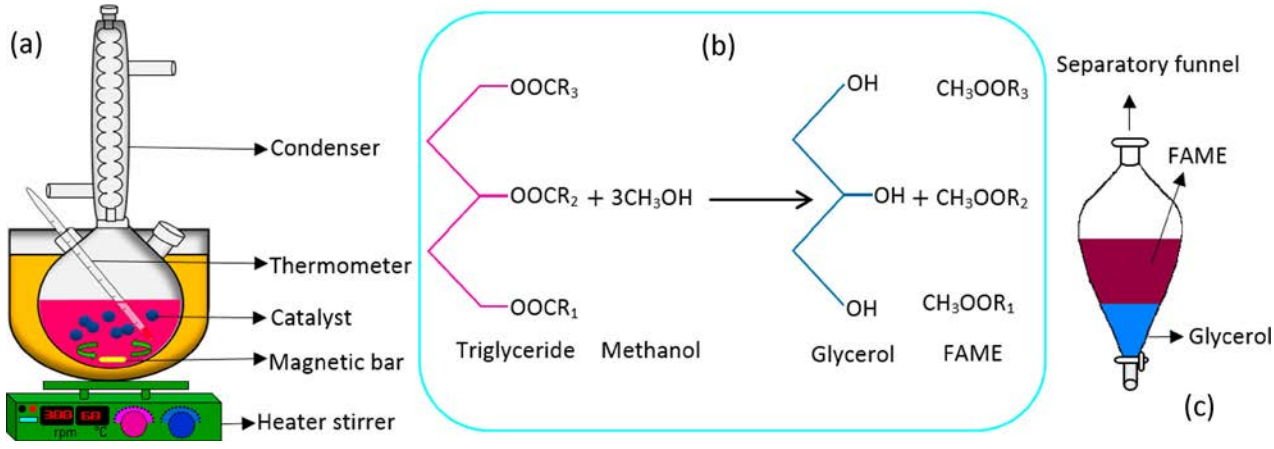

Figure 2. A schematic of the reflux system for WSO trans-esterification with the prepared catalyst and methanol (a), chemistry of biodiesel production (b) and separation of produced biodiesel from glycerol by separatory funnel (c).

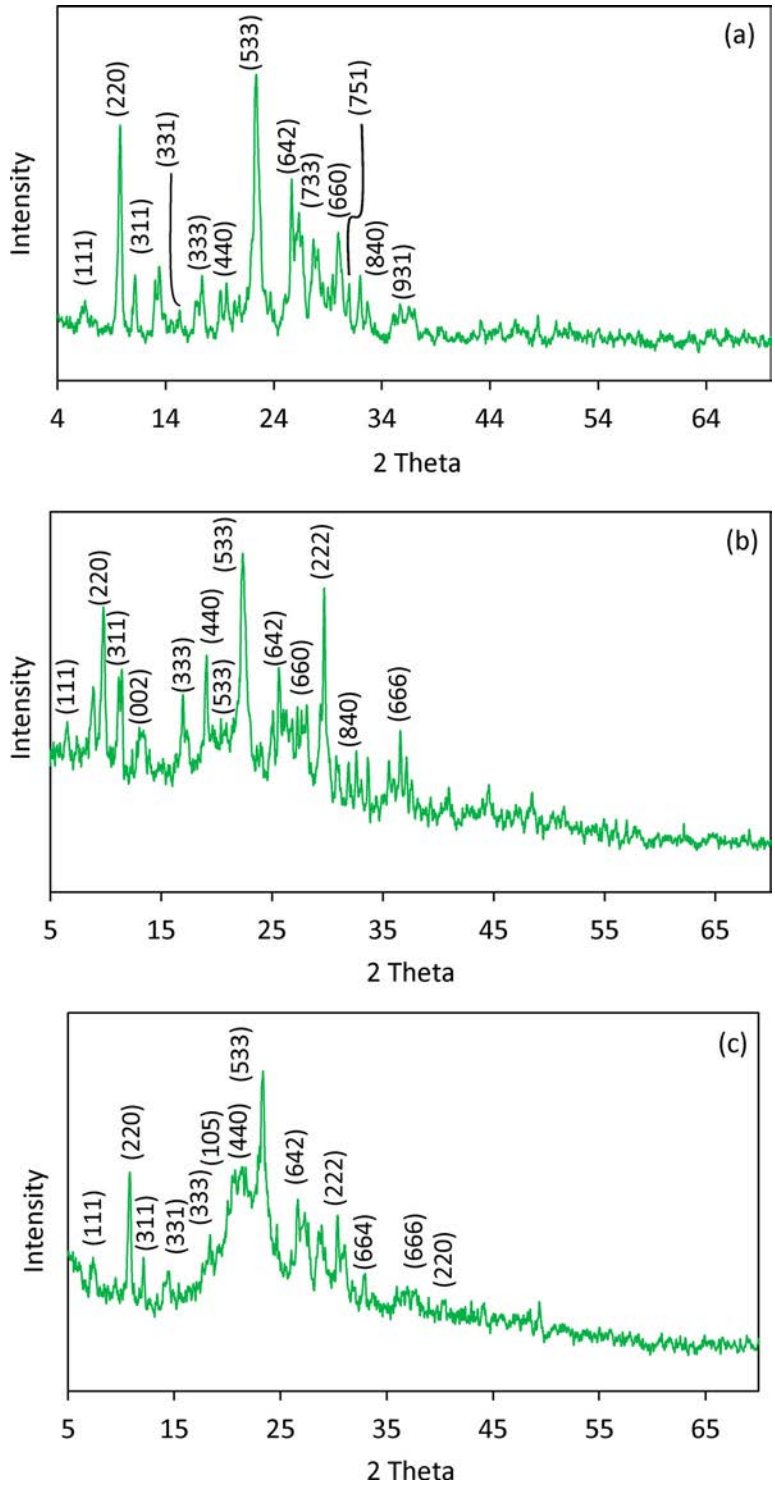

Figure 3. XRD pattern of HSZB (a), prepared catalyst (b) and used catalyst (c).

(0.5, 1, 1.5, 2 and 2.5) and different molar ratio of methanol:oil (3:1, 6:1, 9:1 and 12:1) were added to the oil. Different weight percent of the co-solvent (THF) based on the methanol weight percent (5, 10, 15, 20 and 25) were used to homogenize the reaction mixture. Afterwards, the solution went under reaction at 55°C temperature with 300 rpm stirring speed. In the experiment, glycerin was separated from the biodiesel within 2 h, but different periods of time were allocated to complete the process. The temperature of the reflux system is usually determined based on alcohol boiling point which causes an increase in the final conversion percent. In Figure 2, in a 250 mL round bottom flask of reflux system, the waste oil and catalyst with extra

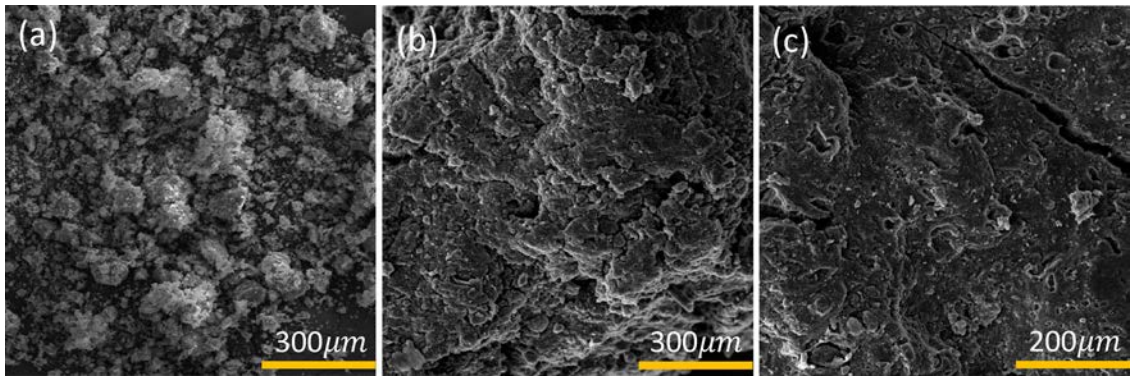

Figure 4. SEM of HSZB (a), prepared catalyst (b) and used catalyst (c).

alcohol were added. After the completion of the trans-esterification reaction, the two glycerol and biodiesel phases were separated and the obtained solution was translocated in the separatory funnel and FAME phase. In the final phase, crude biodiesel should be washed with warm distilled water at 60°C to eliminate impurities and pollutants which may include the remained catalyst, the non-reacted alcohol, glycerol, FFAs or soap. To get rid of the soap from the mixture with high soap formation, stearic acid (0.1%) was added to the flat bottom flask to neutralize and eliminate all formed soap and unreacted K^+. The reaction mixture is washed with distilled water until it becomes fully clear. Washing was done three times in this phase. The extra remained alcohol in this phase should be completely separated with evaporation or distillation. The washed FAME is then dried over sodium sulfate. The following formula was used to calculate biodiesel efficiency (*21*):

$$\text{Yield (\%)} = \frac{\text{weight of the FAME}}{\text{weight of WSO}} \times 100\%. \qquad (3)$$

3. Results and discussion

Figure 3(a,b) displays the XRD used for the inner surface and the structure, solid and crystalline phase of raw Zeolite Beta and modified catalyst. Some species of K_2O may be formed on the zeolite particles' external structure that shows partial distortion of the structure of zeolite due to the occurrence of impregnation step inside the zeolite crystallites. If this happens, some species of K_2O are also formed in the intracrystalline volume or zeolite structure upper cages (*28*). The zeolite peaks intensity decreases with an increase of K that shows an insignificant loss of crystallinity (*29*). Regarding that the existing water in zeolite was removed in the calcination process, KOH was converted to K_2O, as shown in the XRD pattern (*15*,*18*,*30*). Furthermore, two peaks in the (2θ) region = 7° (101) and 22° (302), according to the JCPDS 48-0038 cards and literature data, are attributed to the HSZB phase (*31*). Kusuma et al. showed that the new phase of potassium oxide is emerged at $2\theta = 31°$, 39°, 51°, 55° and 62° (*18*). The K_2O formation strongly indicated that the KOH was well distributed on the surface or structure of HSZB. This is in association with XRD analysis where the structure of zeolite is retained even after treatment alkali (*26*). However, the peak's intensity is low due to high dispersion of K_2O particles. In Figure 3(c), K_2O was used in trans-esterification and washed with alcohol and n-hexane after the process which resulted in the decrease of K_2O in the used catalyst structure in the third cycle.

Figure 4 indicates SEM images of zeolite (a), the prepared catalyst (b) and the used catalyst (c) in the trans-esterification process. Treating the structure of HSZB with KOH agglomerates the pores in zeolite causing the surface of the prepared catalyst seem more integrated that increases the resistance and sustainability of the catalyst. The calcination converts KOH to K_2O as active sites in pores and cages of zeolite (*19*). Alkali metal oxides can enhance the number of basic sites of the zeolite and the basic strength (*14*). This increase in percentage of conversion is attributed to the higher potassium oxide active sites content in the synthesized catalyst (*15*). Figure 5(b,c) indicates a representative EDX of K on the catalyst and used catalyst. The amount of K element enhanced with the KOH treatment, confirming the existence of K element on HSZB, which is considered a good stability of catalyst since a low amount of K content was leached during three trans-esterification cycles.

BET sorptometer (auto absorb from quantachrome) was used to specify the pore volume and specific structure area of zeolite and catalyst. HSZB having a surface area and high pore volume, as a result of hydrothermal treatment during catalyst synthesis decreases particle

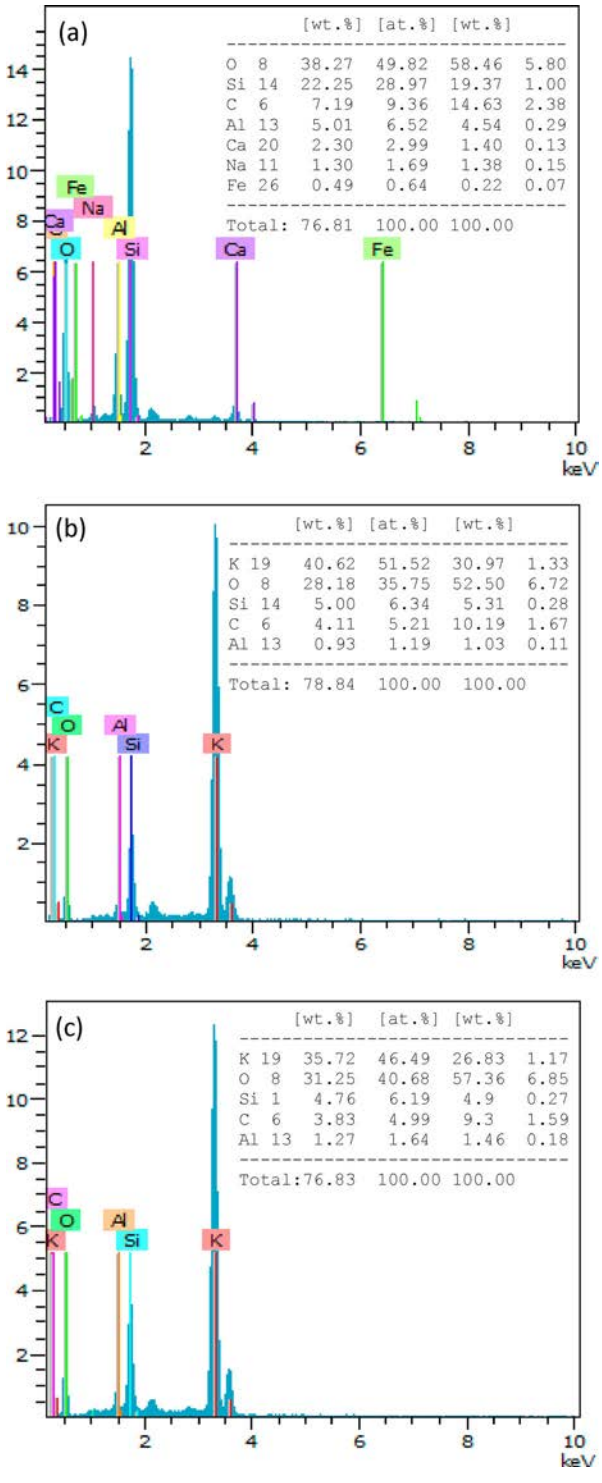

Figure 5. EDX of HSZB (a), prepared catalyst (b) and used catalyst (c).

size. However, total pore volume and catalyst surface area have reduced intensely after a blockage of zeolite surface by K_2O impregnation. Pore diameter average value, on the other hand, has augmented after the process due to zeolite desilication and formation of mesopore. Also, catalyst impregnation by K_2O increases the average pore diameter in spite of the reduced volume of the zeolite beta pores which can be ascribed to blockage of most micropores by K_2O. Accordingly, more free mesopores will be accessible, enhancing pores' average diameter. The total surface area of HSZB was 465.2 $m^2\ g^{-1}$ and the total pore volume was 0.2142 $cm^3\ g^{-1}$. However, the BET surface area and total tore volume values of the catalyst were found to be very low, 34.67 $m^2\ g^{-1}$ and 0.0494 $m^2\ g^{-1}$, respectively, since potassium compounds covered zeolite surface and pores during the impregnation step and a substantial decrease of the pore volume was shown after the impregnation process.

In Figure 6(a), 3432 cm^{-1} shows the sharp band of hydrogen bonded OH, water stretching vibration at 3620 cm^{-1} and the H_2O bending vibration at 1635 cm^{-1}. The band at 3425 cm^{-1} is related to the –O–H stretching and 1640 cm^{-1} is related to bending of adsorbed water. The peak 1348 cm^{-1} in FT-IR related to catalyst shows –O–H deformation vibration of CH_2–OH. The deformation band –Si–O–Si– has a sharp peak at 460 cm^{-1}. However, the –Si–O– exists in the prepared zeolite beta; –Al–OH were observed as a result of zeolite mixing with KOH solution. The SiO_4 and AlO_4 bands at 1021 and 703 cm^{-1} display the asymmetric and symmetric stretching vibrations of the zeolite structure. In HSZB, the wavenumbers in 750–820 cm^{-1} signify the O–M–O (M = Al, Si) symmetric stretching vibration. In Figure 6(b), the rise in the OH groups is a common phenomenon that is associated with the modification of alkaline for the alkaline environments role in the surface of zeolite. A new band at 2874 cm^{-1} was detected that is attributed to hydroxyl groups formed during the modification of alkaline of zeolite precursor by K_2O. The region of vibrational band at 821 cm^{-1} shows the stretching vibrations of K–O group (*32*). Figure 6(c) shows that 675 cm^{-1} is related to –O–Al–O– symmetric stretching. The first two peaks from 721 and 880 cm^{-1} show the used catalyst's impurities. The peak at 1082 cm^{-1} shows asymmetric stretching of –Si–O–Si — and the peak at 1061 cm^{-1} was the carbonate species characteristic peak. In Figure 6(c), the peaks at 3651 and 3413 cm^{-1} were attributed to OH– stretching of Si(OH)Al and the bending vibration of hydroxyl groups of absorbed H_2O at 1644 cm^{-1} (*14*,*20*). After the conversion reactions, the FT-IR spectrum of the used catalyst displayed the main groups with noticeable changes in their positions and intensities as well as the appearance of other new bands. The C–H stretching of $–CH_3$ appeared at 2927 cm^{-1} that is assigned to the methyl or/and methylene groups of methyl esters adsorbed by the catalyst particles. Furthermore, the presence of C=O was established by the observation of the band at 1765 cm^{-1} (*33*).

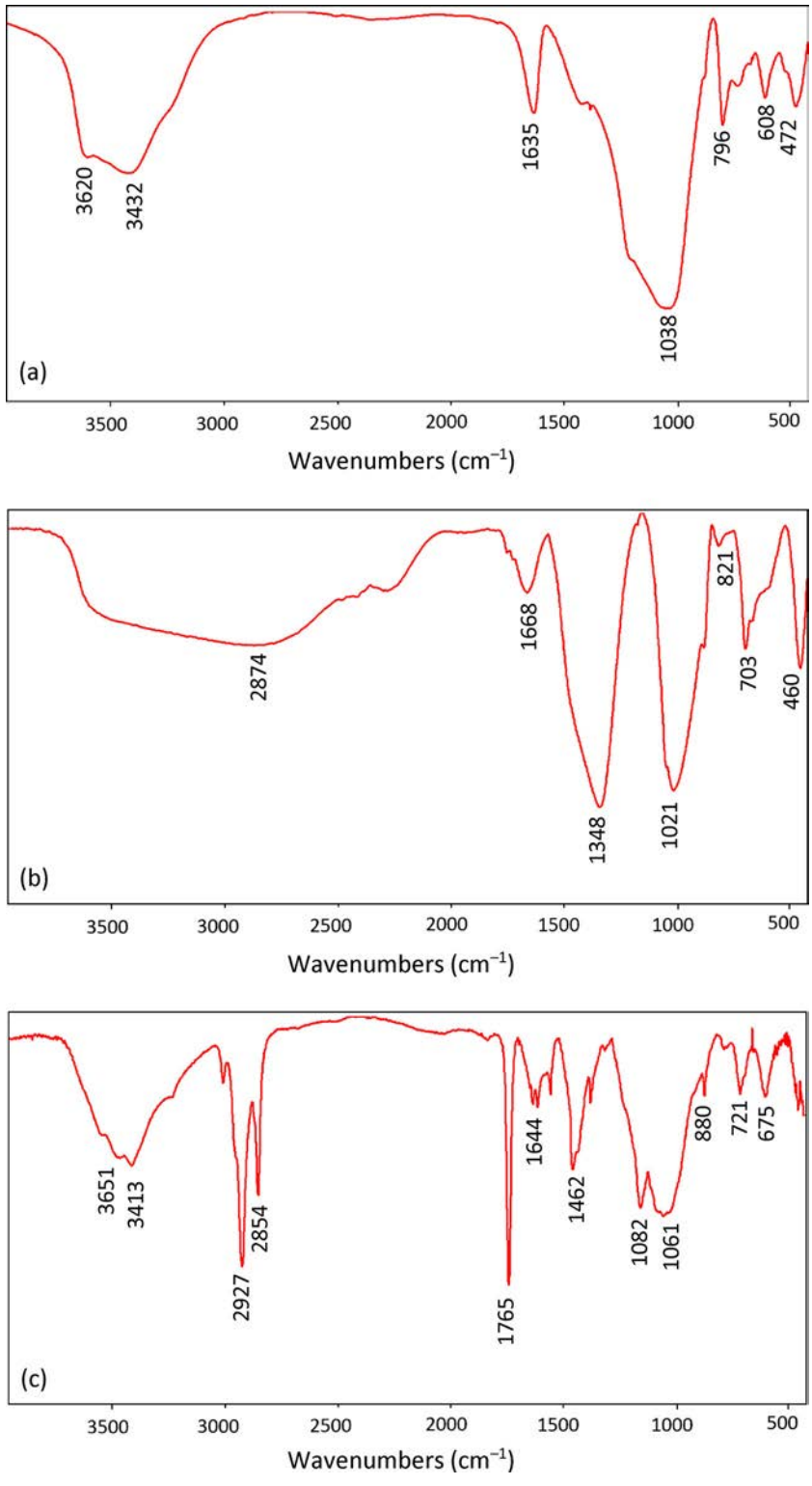

Figure 6. FT-IR spectra of the HSZB (a), prepared catalyst (b) and used catalyst (c).

Figure 7 indicates the effect of alcohol on biodiesel efficiency within a range of 3:1–12:1. Increasing methanol more than the optimized amount does not enhance the reaction which is attributed to the fact that glycerol will be solved partly in the excess methanol consequently to prevent methanol reaction with the catalyst. Sufficient amount of alcohol can enhance the performance of the trans-esterification reaction towards the forward direction and increase the miscibility between the reactant phases (*34*). However, excessive alcohol

has four reversible effects including the deactivation of catalyst, dilution of the present mixture and the associated changes, the possible dissolution of glycerol byproducts and the associated orientation of the reaction to the reversible direction, and the expected changes in the alcohol polar groups which convert the alcohol molecules to be emulsifier centers (*35*). FAME yield of 96.5% was obtained in the presence of alcohol:oil molar ratio of 9:1, 2 wt.% HSZB, co-solvent amount of 20 wt.%. Since methanol was absorbed by HSZB, the optimal methanol:oil molar ratio was higher than 6:1 which is a commonly agreed optimal alcohol:oil ratio in the traditional heterogeneous base catalyzed trans-esterification.

Figure 8 shows the effect of zeolite beta concentration (wt.%) in the trans-esterification reaction within the range of 0.5–2.5 wt.% of catalyst to weight percent of WSO. The conversion reaction has increased from 0.5 to 2 wt.% by the catalyst loading. Figure 8 shows that when catalysis dosage goes more than 2 wt.%, FAME reduces. Optimization of catalyst amount is an important issue in reaching the highest production percent since using excessive catalyst causes saponification of the mixture and formation of gelatinous substance leading to extreme decline of the trans-esterification process. Previous studies and the present research showed that trans-esterification occurs with K_2O catalytic activity and using zeolite, without K_2O as a base catalyst does not lead to trans-esterification (*17*,*21*).

Temperature is one of the most contributing factors in trans-esterification yield. In Figure 9, the temperature

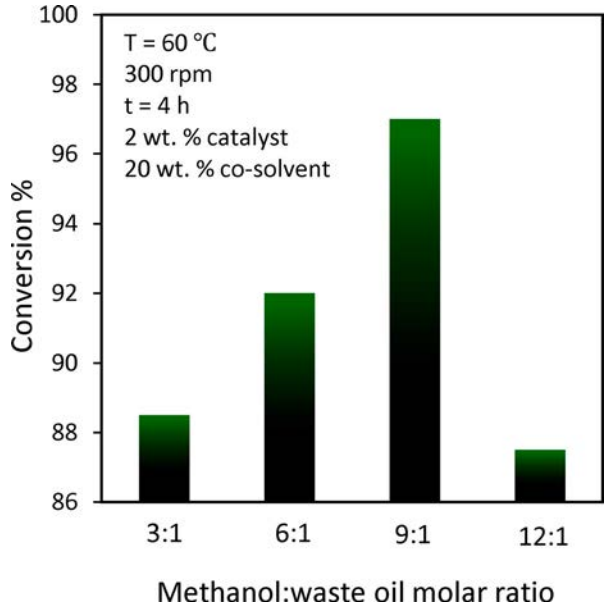

Figure 8. Effect of methanol:waste oil molar ratio on trans-esterification.

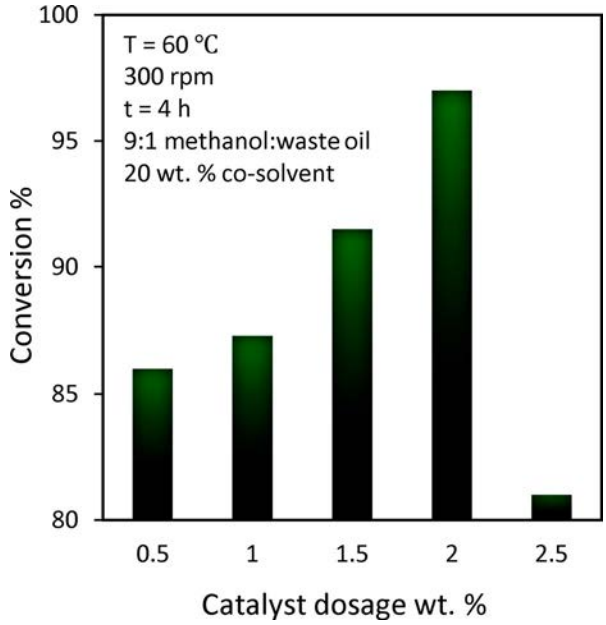

Figure 8. Effect of catalyst dosage on trans-esterification.

range of 25–65°C was considered. The higher the temperature, the lower the viscosity will be to intensify the trans-esterification process. High temperature facilitates the mass transfer between oil and alcohol molecules and consequently increases FAME conversion. It is noteworthy that in Figure 9, the reaction temperature should be a little lower than alcohol boiling point to prevent alcohol evaporation. Because of this, 60°C showed the highest percent of FAME conversion.

Addition of a co-solvent to the trans-esterification reaction makes methanol and waste oil phase mutually

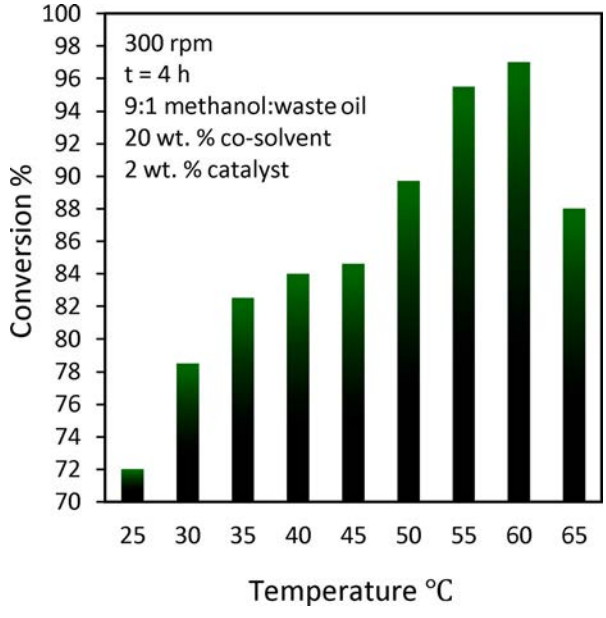

Figure 9. Effect of temperature on trans-esterification.

miscible (*36*). Miscibility of the phases increases the reaction rate due to disappearance of mass transfer resistance between the phases of oil and alcohol (*21*,*37*). Figure 10 shows that for this study, the optimum co-solvent to weight percent (wt.%) of methanol ratio is 20 wt.% producing 96.5% biodiesel yield. It can be concluded that reaction of trans-esterification in the presence of co-solvent takes less time and the purpose of using co-solvent is to reduce energy consumption and time of reaction. As shown in Figure 10, in the absence of co-solvent, the percentage of conversion reduces to 71.5% in the fixed 4 h ($T = 60$°C, 300 rpm, methanol: waste oil molar ratio 9:1, 2 wt.% catalyst). Further increase in the co-solvent ratio lowered the content of FAME probably as a result of the dilution of the reactants. With 25 wt.% of the co-solvent, WSO concentration decreased and consequently reactions decreased (*38*).

Restoring and reusing catalyst is one of the greatest advantages of heterogeneous catalysts (*39*). The catalyst was separated after finalizing and reaching the highest efficiency washed with methanol and n-hexane. This washing allows catalyst's active sites to get rid of molecules which poison these sites. The reduction in conversion percent can be caused by organics deposition inside the molecular sieve which results in active sites decline and active ingredient leaching. At the third run, the zeolite beta deactivates to a certain degree and conversion percent decreases to 66.3% which is caused by leaching of active sites of catalysts structure and obstruction of the active sites during the trans-esterification process (Figure 11).

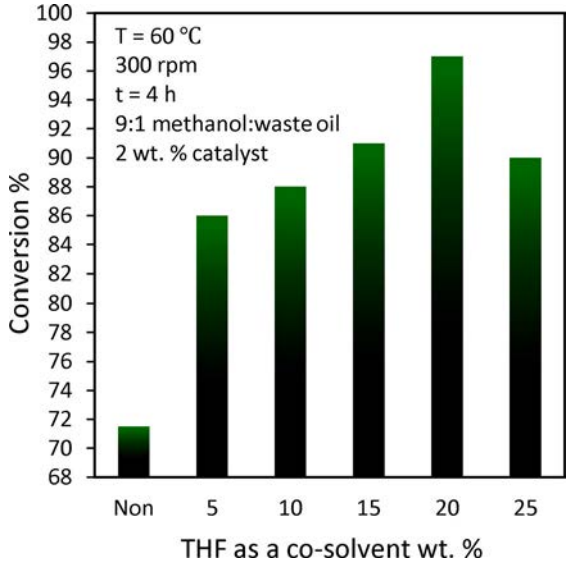

Figure 10. Effect of THF as a co-solvent on trans-esterification.

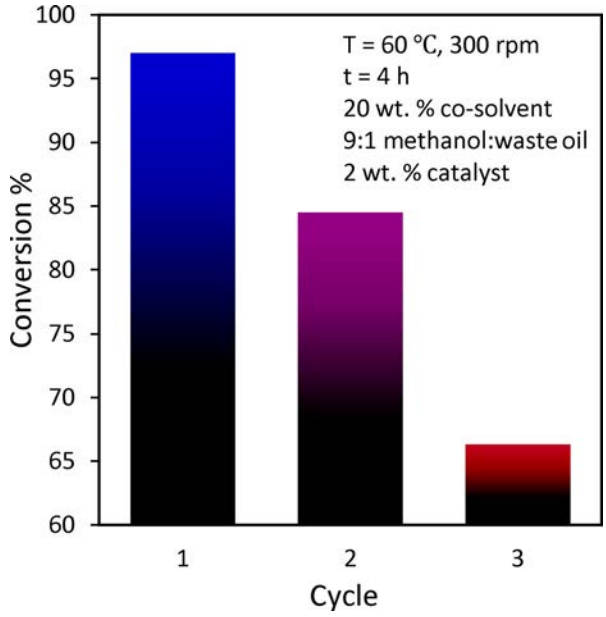

Figure 11. Multiple cycle test of catalyst.

Figure 12(a) shows the characterization properties of the layered structure of catalyst and properties of ion exchange. The structure of the catalyst is mainly composed of an octahedral sheet which is placed between two tetrahedron sheets (*40*). This catalyst has considerable advantages including a structure with many cages and pores, high ion exchange and a wide surface area caused by high porosity. In addition, the activation of alkaline on the surficial siloxane groups leads to hydration of the HSZB sheets. Also, the activation of HSZB by alkaline treatment highly affected the crystal structure of the catalyst. The sharing of the silica tetrahedron structures causes the formation of active sites with cages and pores. The active sites act as traps for K_2O in the activation process of the catalyst surface. Generally, K_2O can be placed within the catalyst structure by partial replacement of ions of aluminum and silicon and as trapped within the interlayer molecules of H_2O. In the presence of water, K_2O can convert into KOH where K^+ converts into active sites for the trans-esterification reaction through blocking the pore openings on the zeolite surface (*29*).

Figure 12(b) displays the trans-esterification reaction mechanism for biodiesel production using HSZB treated with KOH. In the first step of reaction, CH_3O^- ion is formed from the reaction between the active site of K_2O with methanol. This CH_3O^- ion is a strong base which has high catalytic activity in the trans-esterification reaction (*18*). In the second step, the reactive CH_3O^- ion attacks the carbonyl carbon atom of WSO to form tetrahedral intermediate. Further rearrangement of tetrahedral intermediate produced one methyl ester

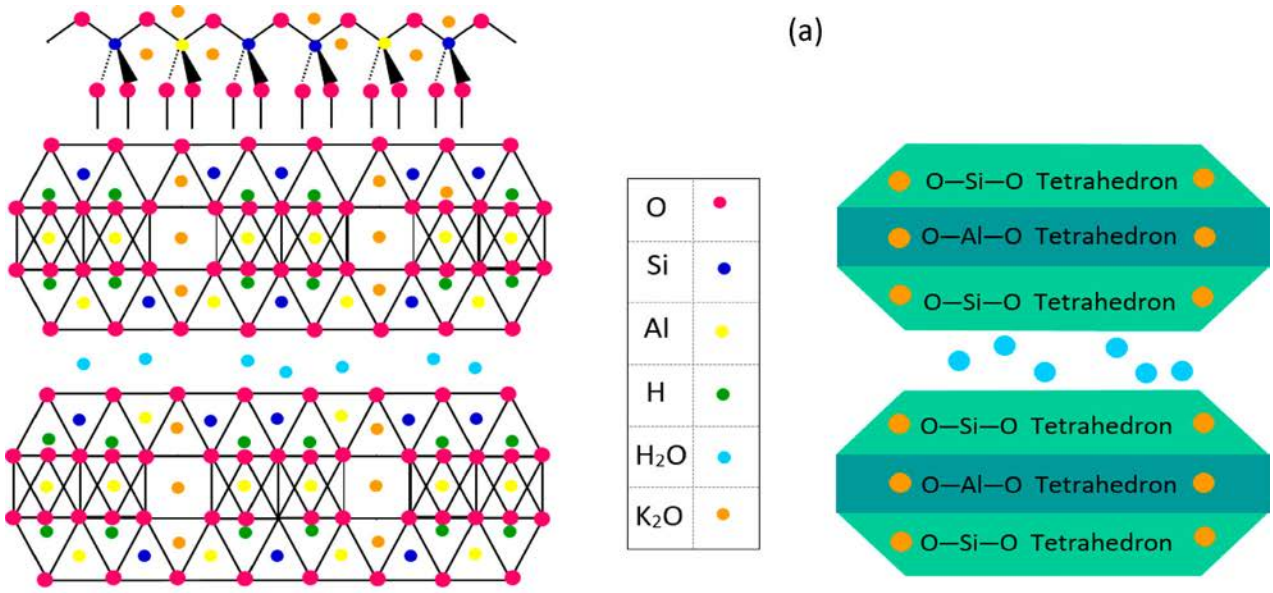

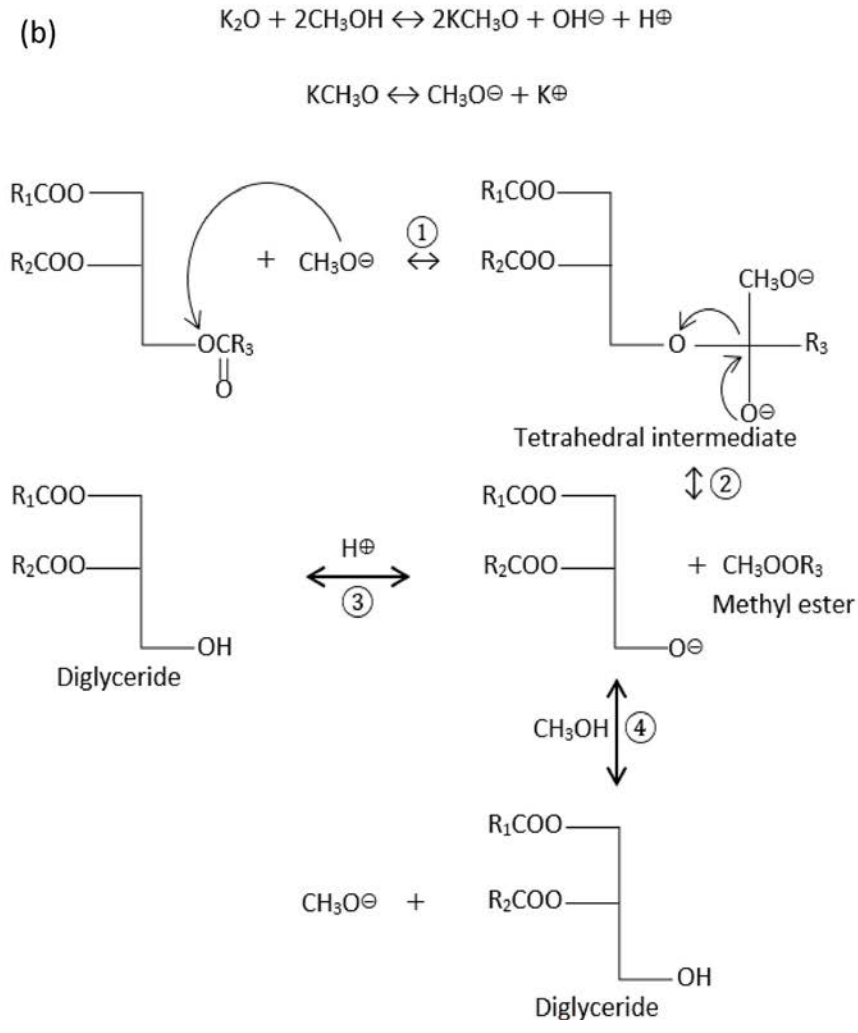

Figure 12. The proposed schematic of the activating HSZB structure by K_2O (a) and reaction mechanism for triglyceride trans-esterification using methanol (b).

Table 1. GC–MS of FAME.

Component		Concentration (%)	Time of retention (min)
Methyl oleate	$C_{19}H_{36}O_2$	0.27	45.49
Methyl lignocerate	$C_{25}H_{50}O_2$	0.78	45.93
Methyl tetradecanoate	$C_{15}H_{30}O_2$	1.09	33.80
Methyl stearate	$C_{19}H_{38}O_2$	7.66	42.70
Methyl palmitate	$C_{17}H_{34}O_2$	37.77	38.84
Methyl oleate	$C_{19}H_{36}O_2$	52.43	42.53

Table 2. Physical properties of FAME.

Property	ASTM D6751 biodiesel	ASTM method	Green diesel
Flash point (°C)	100–170	D 93	150
Pour point (°C)	−15 to 16	D 97	−15
Density (40°C, kg m^{-3})	860–900	D 5002	880
Cloud point (°C)	−3.0 to 12	D 2500	0
Cetane number	45–55	D 613	56

molecule and diglyceride anion. In the third step, diglyceride molecule reconstruction began with the reaction with H^+ from the catalyst. In step 4, the diglyceride anion may also react with methanol and generate reactive CH_3O^- ion. The catalytic reaction was then followed by the reaction between diglyceride and other CH_3O^- ion to produce monoglyceride molecule and one methyl ester molecule. Finally, CH_3O^- ion attacked carbonyl carbon atom of monoglyceride to produce one methyl ester molecule and one glycerol molecule.

Table 1 shows GC–MS of FAME with methyl stearate, methyl palmitate, and methyl oleate as main products. The physical and chemical properties of the produced biodiesel using HSZB including kinematic pour point, cetane number, flash point, density and viscosity were determined by standard analysis as shown in Table 2. Viscosity is an important factor in biodiesel quality so that biodiesel fuel fluidity is directly influenced by its viscosity increase. Injector performance is affected by viscosity. The lower the viscosity, the better the pumping, atomization, and finer droplets achievement. The minimum range of flash point is a necessary condition for handling and fuel safety. Flash point which is very important in preventing liquid explosion and firing hazards should be in the specified standard range. As shown in Table 2, the produced biodiesel flash pint is 150°C. Therefore, it can be concluded that this biodiesel is safe for handling and storage for some period of time. The cetane number of the obtained biodiesel was 56°C which is a little beyond the standard limit. The ignition quality of diesel fuels and the combustion quality of diesel fuel during compression ignition depend on cetane number.

Table 3 shows the comparison of the results of this research with other recent reports of articles on using zeolite as a heterogeneous catalyst in raw materials trans-esterification. It is seen that alkaline catalyst of HSZB is a good alternative in methanolysis of WSO aiming at production of biodiesel.

4. Conclusion

The purpose of this work was to develop an applicable solid catalytic system from HSZB for renewable diesel production from WSO currently attracting increasing attention as an inexpensive feedstock for production of FAME. The suggested catalyst in this study was made from impregnation of HSZB with KOH solution which was converted to K_2O during the calcination process. K_2O as the active catalyst factor has been scattered in the structure pores and surface fractures of

Table 3. Recently reported studies on the trans-esterification reaction using zeolite as a heterogeneous catalyst with different raw materials.

No.	Catalyst	Alcohol	Oil	Reaction time (min)	Temperature (°C)	Yield/conversion (%)	References
1	Natural zeolite from Indonesia/KOH	Methanol	Palm oil	120	60	95.05	(*18*)
2	Zeolite with a high Si/Al ratio/NaOH	Methanol	Triolein	60	65	90	(*41*)
3	Clinoptilolite zeolite/chitosan/KOH	Methanol	Waste cooking oil	180	25	93	(*21*)
4	ZSM5 zeolite/KOH	Methanol	Refined sunflower oil	1440	60	95	(*20*)
5	KOH/ZSM zeolite-5-Fe_3O_4	Methanol	Canola oil	206	65	93.65	(*42*)
6	Bentonite zeolite/NaOH	Methanol	Soybean oil	60	57.8	98.56	(*17*)
7	H-Y and ZSM-5 zeolites	Methanol	Palmitic acid oil	180	70	100	(*43*)
8	High purity FAU-type zeolite	Ethanol	Oleic acid	90	70	78	(*44*)
9	Phosphoric acid modified β-zeolite	Methanol	Pinnai oil	60	60	93	(*45*)
10	Low-Al zeolite beta	Methanol	Triolein	10	65	90	(*46*)
11	Zeolite Na-X from fly ash	Methanol	Sunflower oil	480	65	83.53	(*47*)
12	La^{+3}/zeolite beta	Methanol	Soybean oil	320	60	48.9	(*48*)
13	Zeolite tuff /KOH	Methanol	WSO	120	50	96.7	(*19*)
14	Phosphoric acid modified zeolite	Methanol	Neem oil	60	60	93	(*49*)
15	HSZB/K_2O	Methanol	WSO	240	60	96.5	Present work

HSZB. Proper translocation of K_2O in these sites brings about catalyst stability for reusing. Moreover, the interaction of methanol:waste oil molar ratio and the amount of modified zeolite beta through K_2O and THF as a co-solvent amount were found to have significant effects on conversion of FAME. Addition of a co-solvent to the trans-esterification reaction makes methanol and waste oil phase mutually miscible. The maximum renewable fuel conversion obtained in 4 h reaction time at a temperature of 60°C, co-solvent amount of 20 wt.%, methanol:waste oil molar ratio of 9:1, 2 wt.% catalyst and stirring speed of 300 rpm.

Disclosure statement

No potential conflict of interest was reported by the author(s).

Notes on contributors

Leila Fereidooni is a Ph.D. of Applied Chemistry from Islamic Azad University of Tehran. Her research area focuses on production of biodiesel using renewable resources and green materials to conserve environment.

Dr Mojtaba Enayati is currently a Senior Research Associate of Polymer Chemistry in the Department of Food Science at Cornell University. He will join Troy University as an assistant professor of chemistry in January 2021.

Dr Alireza Abbaspourrad is currently an Assistant Professor of Food Chemistry and Ingredient Technology in the Department of Food Science at Cornell University.

References

[1] Akinfalabi, S.-I.; Rashid, U.; Ngamcharussrivichai, C.; Nehdi, I.A. *Environ. Technol. Innov.* **2020**, *18*, 100788.

[2] Kanitkar, A.; Balasubramanian, S.; Lima, M.; Boldor, D. *Bioresour. Technol.* **2011,** *102* (17), 7896–7902.

[3] Kaimal, V.K.; Vijayabalan, P. *J. Energy Inst.* **2017,** *90* (2), 324–330.

[4] Dehghani, S.; Haghighi, M.; Vardast, N. *Int. J. Energy Res.* **2019,** 43, 3779– 3793.

[5] Fereidooni, L.; Pirkarami, A. *Phys. Chem. Res.* **2019,** *7* (3), 491–498.

[6] Fereidooni, L.; Tahvildari, K.; Mehrpooya, M. *Renew. Energy* **2018,** *116* (Part A), 183–193.

[7] Cherikkallinmel, S.K.; Sugunan, S.; Narayanan, B.N.; Faisal, P.A.; Benjamin, S. *Korean J. Chem. Eng.* **2017,** 34, 2840–2851.

[8] Abu-Jrai, A.M.; Jamil, F.; Al-Muhtaseb, A.a.H.; Baawain, M.; Al-Haj, L.; Al-Hinai, M.; Al-Abri, M.; Rafiq, S. *Energy Convers. Manage.* **2017,** *135*, 236–243.

[9] Fereidooni, L.; Khalilnezhad, R.; Pirkarami, A. *Phys. Chem. Res.* **2018,** *6* (2), 323–333.

[10] Bhatia, S.K.; Gurav, R.; Choi, T.-R.; Kim, H.J.; Yang, S.-Y.; Song, H.-S.; Park, J.Y.; Park, Y.-L.; Han, Y.-H.; Choi, Y.-K.; Kim, S.-H.; Yoon, J.-J.; Yang, Y.-H. *Bioresour. Technol.* **2020,** *302*, 122872.

[11] Jamil, M.A.R.; Touchy, A.S.; Poly, S.S.; Rashed, Md.N.; Siddiki, S.M.A.H.; Toyao, T.; Maeno, Z.; Shimizu, K.-i. *Fuel Process. Technol.* **2020,** *197*, 106204.

[12] Jacobs, P.; Flanigen, E.M.; Jansen, J.; Bekkum, H. van. *Introduction to Zeolite Science and Practice*, vol. 137; Elsevier: Amsterdam, 2001.

[13] Moshoeshoe, M.; Nadiye-Tabbiruka, M.S.; Obuseng, V. *Am. J. Mater. Sci.* **2017,** *7* (5), 196–221.

[14] Supamathanon, N.; Khabuanchalad, S. *Mater. Today: Proc.* **2019,** *17*, 1412–1422.

[15] Soetaredjo, F.E.; Ayucitra, A.; Ismadji, S.; Maukar, A.L. *Appl. Clay Sci.* **2011,** *53* (2), 341–346.

[16] Wu, L.; Wei, T.-y.; Tong, Z.-f.; Zou, Y.; Lin, Z.-j.; Sun, J.-h. *Fuel Process. Technol.* **2016,** *144*, 334–340.

[17] Wu, L.; Wei, T.; Lin, Z.; Zou, Y.; Tong, Z.; Sun, J. *Fuel* **2016**, *182,* 920–927.

[18] Kusuma, R.I.; Hadinoto, J.P.; Ayucitra, A.; Soetaredjo, F.E.; Ismadji, S. *Appl. Clay Sci.* **2013,** *74*, 121–126.

[19] Al-Jammal, N.; Al-Hamamre, Z.; Alnaief, M. *Renew. Energy* **2016,** *93*, 449–459.

[20] Saba, T.; Estephane, J.; El Khoury, B.; El Khoury, M.; Khazma, M.; El Zakhem, H.; Aouad, S. *Renew. Energy* **2016,** *90*, 301–306.

[21] Fereidooni, L.; Mehrpooya, M. *Energy Convers. Manage.* **2017,** *147*, 145–154.

[22] Cheng, Z.-L.; Li, Y.-X.; Liu, Z. *J. Alloys Compd.* **2017**, *708* (Supplement C), 255–263.

[23] Kim, H.-J.; Kang, B.-S.; Kim, M.-J.; Park, Y.M.; Kim, D.-K.; Lee, J.-S.; Lee, K.-Y. *Catal. Today* **2004,** *93–95*, 315–320.

[24] Tanawannapong, Y.; Kaewchada, A.; Jaree, A. *J. Ind. Eng. Chem.* **2013**, *19* (1), 37–41.

[25] Harsha, H.H.R.; Math, M.C.; Yatish, K.V. *Energy* **2018**, *143*, 25–34.

[26] Muciño, G.E.G.; Romero, R.; García-Orozco, I.; Serrano, A.R.; Jiménez, R.B.; Natividad, R. *Catal. Today* **2016**, *271*, 220–226.

[27] Hassani, M.; Najafpour, G.D.; Mohammadi, M.; Rabiee, M. JSIR **2014,** *73* (02),129–133.

[28] Kikhtyanin, O.; Ganjkhanlou, Y.; Kubička, D.; Bulánek, R.; Čejka, J. *Appl. Catal. A* **2018**, *549*, 8–18.

[29] Intarapong, P.; Iangthanarat, S.; Phanthong, P.; Luengnaruemitchai, A.; Jai-In, S. *J. Energy Chem.* **2013**, *22* (5), 690–700.

[30] Noiroj, K.; Intarapong, P.; Luengnaruemitchai, A.; Jai-In, S. *Renew. Energy* **2009,** *34* (4), 1145–1150.

[31] Treacy, M.M.; Higgins, J.B.; von Ballmoos, R. *Zeolites* **1996,** *16* (5–6), 478.

[32] Abukhadra, M.R.; Salam, M.A.; Ibrahim, S.M. *Renew. Sustain. Energy Rev.* **2019,** *115*, 109346.

[33] Abukhadra, M.R.; Sayed, M.A. *Energy Convers. Manage.* **2018,** *177*, 468–476.

[34] Rabie, A.M.; Shaban, M.; Abukhadra, M.R.; Hosny, R.; Ahmed, S.A.; Negm, N.A. *J. Mol. Liq.* **2019,** *279*, 224–231.

[35] Abukhadra, M.R.; Dardir, F.M.; Shaban, M.; Ahmed, E.A.; Soliman, M.F. *Environ. Chem. Lett.* **2018,** *16* (2), 665–670.

[36] Guan, G.; Sakurai, N.; Kusakabe, K. *Chem. Eng. J.* **2009,** *146* (2), 302–306.

[37] Rahimi, M.; Mohammadi, F.; Basiri, M.; Parsamoghadam, M.A.; Masahi, M.M. *J. Taiwan Inst. Chem. Eng.* **2016,** *64*, 203–210.

[38] Hájek, M.; Vávra, A.; Mach, P.; Straková, A. *J. Environ. Manage.* **2020,** *262*, 110295.

[39] Fereidooni, L.; Pirkarami, A. *Phys. Chem. Res.* **2018,** *6* (4), 805–814.
[40] Nakai, M.; Miyake, K.; Inoue, R.; Ono, K.; Al Jabri, H.; Hirota, Y.; Uchida, Y.; Miyamoto, M.; Nishiyama, N. *Microporous Mesoporous Mater.* **2019,** *273*, 189–195.
[41] Wang, Y.-Y.; Chen, B.-H. *Catal. Today* **2016**, *278* (Part 2), 335–343.
[42] Rezayan, A.; Taghizadeh, M. *Process Saf. Environ. Protect.* **2018,** *117*, 711–721.
[43] Prinsen, P.; Luque, R.; González-Arellano, C. *Microporous Mesoporous Mater.* **2018**, *262* (Supplement C), 133–139.
[44] Doyle, A.M.; Alismaeel, Z.T.; Albayati, T.M.; Abbas, A.S. *Fuel* **2017,** *199*, 394–402.
[45] SathyaSelvabala, V.; Selvaraj, D.K.; Kalimuthu, J.; Periyaraman, P.M.; Subramanian, S. *Bioresour. Technol.* **2011,** *102* (2), 1066–1072.
[46] Wang, Y.-Y.; Lee, D.-J.; Chen, B.-H. *Energy Procedia* **2014,** *61*, 918–921.
[47] Babajide, O.; Musyoka, N.; Petrik, L.; Ameer, F. *Catal. Today* **2012,** *190* (1), 54–60.
[48] Shu, Q.; Yang, B.; Yuan, H.; Qing, S.; Zhu, G. *Catal. Commun.* **2007,** *8* (12), 2159–2165.
[49] SathyaSelvabala, V.; Varathachary, T.K.; Selvaraj, D.K.; Ponnusamy, V.; Subramanian, S. *Bioresour. Technol.* **2010,** *101* (15), 5897–5902.